Pediatric Radiology (2019) 49:876–888
https://doi.org/10.1007/s00247-019-04384-7

ORIGINAL ARTICLE

Free-breathing 3-D quantification of infant body composition and hepatic fat using a stack-of-radial magnetic resonance imaging technique

Tess Armstrong [1,2] · Karrie V. Ly [3,4] · Shahnaz Ghahremani [1] · Kara L. Calkins [3] · Holden H. Wu [1,2]

Received: 9 October 2018 / Revised: 12 February 2019 / Accepted: 8 March 2019 / Published online: 17 April 2019

Abstract

Background Body composition and hepatic fat correlate with future risk for metabolic syndrome. In children, many conventional techniques for quantifying body composition and hepatic fat have limitations. MRI is a noninvasive research tool to study body composition and hepatic fat in infants; however, conventional Cartesian MRI is sensitive to motion, particularly in the abdomen because of respiration. Therefore we developed a free-breathing MRI technique to quantify body composition and hepatic fat in infants.

Objective In infants, we aimed to (1) compare the image quality between free-breathing 3-D stack-of-radial MRI (free-breathing radial) and 3-D Cartesian MRI in the liver and (2) determine the feasibility of using free-breathing radial MRI to quantify body composition and hepatic proton-density fat fraction (PDFF).

Materials and methods Ten infants ages 2–7 months were scanned with free-breathing radial (two abdominal; one head and chest) and Cartesian (one abdominal) MRI sequences. The median preparation and scan times were reported. To assess feasibility for hepatic PDFF quantification, a radiologist masked to the MRI technique scored abdominal scans for motion artifacts in the liver using a 3-point scale (1, or non-diagnostic, to 3, or no artifacts). Median visceral adipose tissue (VAT), subcutaneous adipose tissue (SAT) and brown adipose tissue (BAT) volume and PDFF, and hepatic PDFF were measured using free-breathing radial MRI. We assessed repeatability of free-breathing radial hepatic PDFF (coefficient of repeatability) between back-to-back scans. We determined differences in the distribution of image-quality scores using McNemar-Bowker tests. $P<0.05$ was considered significant.

Results Nine infants completed the entire study (90% completion). For ten infants, the median preparation time was 32 min and scan time was 24 min. Free-breathing radial MRI demonstrated significantly higher image-quality scores compared to Cartesian MRI in the liver (radial scan 1 median = 2 and radial scan 2 median = 3 vs. Cartesian median = 1; $P=0.01$). Median measurements using free-breathing radial were VAT=52.0 cm^3, VAT-PDFF=42.2%, SAT=267.7 cm^3, SAT-PDFF=87.1%, BAT=1.4 cm^3, BAT-PDFF=26.1% and hepatic PDFF=3.4% (coefficient of repeatability <2.0%).

Conclusion In this study, free-breathing radial MRI in infants achieved significantly improved liver image quality compared to Cartesian MRI. It is feasible to use free-breathing radial MRI to quantify body composition and hepatic fat in infants.

Keywords Body composition · Free-breathing · Infant · Magnetic resonance imaging · Proton-density fat fraction · Radial magnetic resonance imaging

✉ Holden H. Wu
holdenwu@mednet.ucla.edu

[1] Department of Radiological Sciences,
University of California Los Angeles,
300 UCLA Medical Plaza, Ste. B119, Los Angeles, CA 90095, USA

[2] Physics and Biology in Medicine,
University of California Los Angeles,
Los Angeles, CA, USA

[3] Department of Pediatrics, Division of Neonatology,
David Geffen School of Medicine,
University of California Los Angeles, Mattel Children's Hospital,
Los Angeles, CA, USA

[4] Physician Assistant Program, Midwestern University,
Glendale, AZ, USA

Introduction

The pediatric obesity epidemic and rising rates of metabolic syndrome [1] are critical health issues. Metabolic syndrome is a collection of conditions [2–4], including insulin resistance, dyslipidemia and cardiovascular disease, and it is associated with non-alcoholic fatty liver disease (NAFLD) [2–8], which is characterized by hepatic steatosis [7–9]. Analysis of body composition, especially the amount, distribution and content of adiposity, is important for studying metabolic syndrome

and associated diseases. Fat can be characterized as either white adipose tissue (WAT) or brown adipose tissue (BAT). WAT stores triglycerides while BAT metabolizes fat to produce heat [10]. In the abdomen, WAT is categorized as either visceral adipose tissue (VAT), located inside the abdominal cavity, or subcutaneous adipose tissue (SAT), located outside the abdominal cavity [10]. BAT is generally located in the axillary, supraclavicular, cervical, paravertebral, perirenal and periadrenal regions [10]. Tissue fat content is related to the proportion of different types of fat; higher fat content may indicate "WAT-like" tissue and lower fat content may be associated with "BAT-like" tissue [11–13]. Excess VAT can increase the risk for obesity, metabolic syndrome and NAFLD [10, 14, 15], whereas BAT might protect against obesity [10, 12, 13, 16]. In addition, ectopic organ fat, such as hepatic steatosis, is associated with an increased risk for metabolic syndrome [3, 5, 6].

Evidence shows that events during fetal life and early childhood play a central role in the pathogenesis of obesity and metabolic syndrome [17–19]. Therefore, knowledge about body composition during infancy is important for understanding the early origins of obesity and metabolic syndrome. Infants born to obese mothers with and without gestational diabetes have increased hepatic fat, a potential biomarker for future metabolic diseases [20, 21]. However, current techniques for analyzing body composition and hepatic fat in infants have limitations. The gold standard for body composition analysis is measurement in cadavers [22, 23]. These studies are time-consuming and complex and do not support longitudinal in vivo monitoring [22]. Computed tomography (CT) and dual-energy X-ray absorptiometry are noninvasive imaging techniques for body composition analysis [14] but involve radiation [22, 24]. While ultrasound is a noninvasive and non-ionizing imaging tool that has been used to measure body composition and hepatic fat, it is operator-dependent, has poor resolution, reproducibility and accuracy [22, 25], and becomes unreliable in deeper regions of the body [22]. The gold standard for quantifying hepatic fat is a liver biopsy [7, 9, 26]; however, biopsies are invasive, limited by sampling bias, and have complications [26].

Magnetic resonance techniques, such as magnetic resonance imaging (MRI) and magnetic resonance spectroscopy (MRS), are noninvasive and can be used for longitudinal studies. MRI and MRS are well suited for children because they do not involve ionizing radiation [22, 27]. MRS is regarded as the noninvasive reference standard for quantifying hepatic fat content in children and adults [28–30]. However, MRS techniques have limitations because of partial volume effects, spatial sampling bias, and motion. MRS techniques only measure fat content in a specified voxel and do not provide information about fat distribution. In contrast, MRI has excellent soft-tissue contrast and can obtain high-resolution 3-D images [22, 27]. Intensity-based MRI techniques can provide spatially resolved information about fat distribution and volume in infants [15, 20, 21, 31, 32], but they do not provide information about fat content. Chemical-shift-encoded MRI techniques can provide spatially resolved information about fat distribution, volume and content [11, 32] by quantifying proton-density fat fraction (PDFF), a standardized MRI biomarker [33].

Conventional MRI scans are performed using Cartesian sampling [11–13, 15, 16, 20, 21, 31, 32, 34–36], which is limited by sensitivity to motion-induced coherent aliasing artifacts that can obstruct the anatomy of interest, degrade image quality in organs affected by motion, and hinder quantification. Therefore, scans using Cartesian trajectories are typically performed while breath-holding. However, infants cannot breath-hold, breathe heavily and irregularly, and might cry during the MRI exam. This leads to motion artifacts and non-diagnostic images [37–40]. To improve image quality for clinical infant scans, sedation or anesthesia can be prescribed. However, sedation or anesthesia is not feasible in a research setting or for body composition analysis [37–40]. Because of the lack of age-appropriate technology, a limited number of MRI studies have investigated VAT, SAT, BAT and hepatic fat in infants [11, 12, 15, 16, 20, 21, 31, 34–36].

Compared to Cartesian MRI, non-Cartesian MRI based on 3-D stack-of-radial sampling might provide greater robustness to motion because of the dispersed distribution of motion artifacts [41, 42]. The 3-D stack-of-radial trajectory allows for considerably less obtrusive motion artifacts that do not obscure the anatomy of interest, allowing the MRI scan to be performed during free-breathing [42, 43]. A recently developed free-breathing 3-D stack-of-radial MRI fat quantification technique (free-breathing radial) demonstrated agreement with conventional breath-held Cartesian MRI and reference breath-held MRS in a fat phantom and in the abdomen of healthy adults and older children [42, 43]. In our pediatric study, free-breathing radial MRI produced high-quality images and achieved accurate and repeatable hepatic fat quantification compared to conventional breath-held Cartesian MRI and reference breath-held MRS [43]. We believe the capabilities of free-breathing radial MRI can be extended to quantify body composition and hepatic fat in infants. Hence, this study's purpose was to (1) compare the image quality of free-breathing radial MRI [42] to that of conventional Cartesian MRI in the liver and (2) evaluate the feasibility of the free-breathing radial MRI technique [42] to quantify body composition and hepatic fat in infants.

Materials and methods

Infant study population

This study was approved by our institutional review board. All procedures performed in studies involving human participants

were in accordance with the ethical standards of the institutional and national research committees and with the 1964 Helsinki declaration and its later amendments, or comparable ethical standards.

Parents/legal guardians provided informed consent. Healthy infants ages 1–12 months were eligible for participation. Exclusion criteria included known liver diseases, infections that affect the liver (e.g., toxoplasmosis, rubella, cytomegalovirus, human immunodeficiency virus or herpes simplex virus), major congenital anomalies or diseases that involve the liver, inborn errors of metabolism, and contraindications for MRI.

Infant preparation and magnetic resonance imaging experiments

Preparation and scanning procedures were adapted from previous recommendations [37–40]. See the Appendix for a detailed description of the preparation and scanning procedures. Preparation time for the MRI scan began when the infant entered the MRI suite and included feeding, swaddling and rocking the infant until he or she became sleepy. Earplugs and earmuffs (MiniMuffs; Natus Medical, Pleasanton, CA) were placed on the infant's ears for hearing protection (Fig. 1). Next, infants were placed on a vacuum immobilizer (MedVac; CFI Medical, Fenton, MI) and clips were fastened on the immobilizer (Fig. 1). Air was not removed from the vacuum immobilizer. The infant was placed on the posterior portion of the head array coil at this time (Fig. 1). Finally, the anterior portion of the head coil was attached (Fig. 1). If the infant cried, the anterior portion of the head coil was removed. After all of the coils were positioned and the infant was calm, the MRI table and infant were advanced into the MRI bore and the total preparation time was recorded. An example of the infant preparation procedures is shown in Fig. 1.

After advancing the table and infant into the MRI bore, the start time for the scan was recorded. If the infant cried during the first MRI scan and did not stop crying or the parent/legal guardian requested to stop the scan, the infant was removed from the scanner and comforted in the immobilizer. If the infant settled down, the infant was placed on the MRI table again and set-up procedures on the MRI table were repeated (Fig. 1). The total scan time was calculated after the MRI scan protocol was completed.

The infant MRI experiments were performed on a 3-tesla (T) scanner (Magnetom Skyra or Prisma; Siemens Healthineers, Erlangen, Germany) using a 20-channel head array coil, 32-channel spine array coil and 18-channel body matrix array. A free-breathing radiofrequency-spoiled bipolar multi-echo gradient-echo 3-D stack-of-radial sequence with golden angle ordering [41] and gradient error and eddy current correction [42] (free-breathing radial) was used to acquire abdominal and head and chest scans. The 3-D slabs for the head and chest scan were prescribed to overlap slightly with the abdominal scan for each infant, to cover the body contiguously. Free-breathing radial abdominal scans were repeated back-to-back to assess intra-session repeatability (scan 1 and scan 2). We acquired a commercially available radiofrequency-

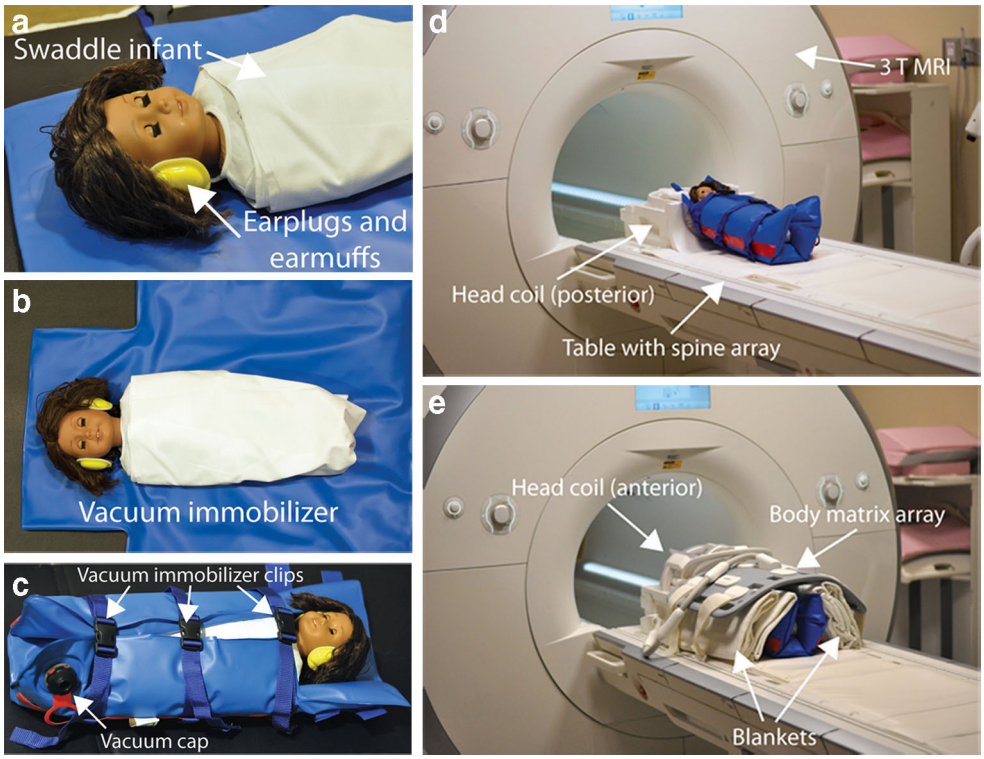

Fig. 1 Infant MRI procedures. **a–c** Initial preparation for the infant scan. **a** First, feed and swaddle the infant and apply hearing protection. **b** Next, place the infant on the vacuum immobilizer. **c** Finally, fasten the vacuum immobilizer clips. Air was not removed from the vacuum immobilizer. **d–e** Preparation on the MRI table. **d** Place the infant on the table with the posterior head coil. **e** Next, add blankets on either side of the infant to prop up the body matrix array. Finally, position the body matrix array and the anterior head coil

spoiled bipolar multi-echo gradient-echo 3-D Cartesian sequence [44] with four-fold undersampling and controlled aliasing in parallel imaging results in higher acceleration (CAIPIRINHA) [45] reconstruction (qDixon; The Liver Lab, software version VE11, Siemens Healthineers, Erlangen, Germany). All scans were performed without breath-holding or sedation. Imaging parameters for the free-breathing radial and Cartesian scans are reported in Table 1.

Magnetic resonance image reconstruction and proton-density fat fraction calculation

Free-breathing radial images and PDFF maps were generated offline in MATLAB version R2017b (MathWorks, Natick, MA). Free-breathing radial images were reconstructed fully sampled (according to the Nyquist criteria) using gradient and eddy current correction [42], linear density compensation, gridding and adaptive coil combination. PDFF maps were determined by fitting the multiple-echo-time images to the gradient-echo signal model with multiple fat peaks [46] to solve for the field map, single effective R_2*, water-only, and fat-only maps with complex fitting using a graph cut algorithm [47–49]. Magnitude discrimination was used to minimize noise bias to calculate PDFF maps from the water- and fat-only images [50]. Cartesian MR images and PDFF maps were calculated on the scanner using a prototype reconstruction method with the same signal model (prototype version 963, qDixon; The Liver Lab, Software version VE11, Siemens Healthineers, Erlangen, Germany).

Liver image quality analysis

All reconstructed images and PDFF maps were converted to Digital Imaging and Communications in Medicine (DICOM) format for analysis in OsiriX software version 6.0 (Pixmeo SARL, Bernex, Switzerland). Image quality was evaluated by an experienced pediatric radiologist (S.G., >10 years of experience), who was blinded to the trajectory (Cartesian or radial) on a scale of 1–3 for motion artifacts. The criteria for a score of 1 was non-diagnostic images with significant artifacts in the liver (i.e. bad image quality); 2 indicated minor motion artifacts in the liver; 3 indicated no motion artifacts in the liver (i.e. good image quality). We determined the percentage of images that fell into each score category.

Body composition analysis

Fat composition was defined as VAT, SAT and BAT volumes (cm^3). Fat content was defined as the PDFF (0–100%). Body composition was measured and analyzed in Horos software version 3 (The Horos Project, horosproject.org). The VAT, SAT and BAT were segmented using the 2-D region growing segmentation and brush tools on the free-breathing radial PDFF maps (all slices in the 3-D volume). VAT was defined

Table 1 Imaging parameters for infant abdominal, and head and chest MRI scans

Imaging parameters	Cartesian, abdomen	Free-breathing radial, abdomen	Free-breathing radial, head and chest
TE (ms)	1.23, 2.46, 3.69, 4.92, 6.15, 7.38	1.23, 2.46, 3.69, 4.92, 6.15, 7.38	1.23, 2.46, 3.69, 4.92, 6.15, 7.38
ΔTE (ms)	1.23	1.23	1.23
TR (ms)	8.85	8.85	8.85
Matrix (N_x×N_y)	96–128×96–128	96–128×96–128	128–160×128–160
Field of view (mm_x×mm_y)	150–200×150–200	150–200×150–200	200–250×200–250
Resolution (mm_x×mm_y)	1.56×1.56	1.56×1.56	1.56×1.56
Number of slices	40	40–44	60–80
Slice thickness (mm)	3	3	3
Bandwidth (Hz/pixel)	1,150–1,155	1,150–1,155	1,150–1,155
Flip angle (degrees)	5	5	5
Radial spokes	N/A	151–202[a]	202–252[a]
Acceleration factor	4	1	1
Scan time (min:s)	0:11–0:14	1:38–2:10[b]	3:20–4:43[c]

All acquisitions used 20–25% slice oversampling. Cartesian scans were acquired without breath-holding. Free-breathing radial abdominal scans were acquired twice to assess repeatability

[a] The number of spokes was adjusted to acquire fully sampled data based on Nyquist sampling criteria (i.e. number of radial spokes = $N_x \times \pi/2$)

[b] Includes gradient calibration acquisition time of 34–37 s

[c] Includes gradient calibration acquisition time of 51–68 s

min minutes, *s* seconds, *TE* echo time, *TR* repetition time

as adipose tissue in the intra-abdominal area [27, 32]. SAT was defined as adipose tissue above the muscle fascia and below the skin in the abdomen [27]. VAT and SAT were subjectively delineated on all abdominal axial slices avoiding blood vessels, bones, intramuscular fat and organs [27, 32]. BAT was analyzed on three consecutive reformatted coronal slices of the supraclavicular region [12, 16, 36]. Areas of BAT were defined as any accumulation of adiposity in the supraclavicular area found in the lower neck and the axillary regions [12, 16, 36]. The number of slices and time to contour all the slices to determine VAT, SAT and BAT for each subject was recorded and was reported as median ± interquartile range. All of the segmented areas of VAT, SAT and BAT on the PDFF maps were summed per pixel count to compute the volume and mean PDFF in each subject. All body composition measurements were performed by the same study coordinator (K.V.L.) for consistency. All slices and segmentations were reviewed and confirmed by a pediatric radiologist (S.G., >10 years of experience).

Hepatic fat quantification

Hepatic fat was measured on a single 15mm × 15mm × 15mm region of interest encompassing five 3-mm slices on free-breathing radial PDFF maps. These regions of interest were placed to avoid large blood vessels and bile ducts and in anatomically corresponding regions in the liver to reduce variations in position caused by motion. A pediatric radiologist (S.G., >10 years of experience) confirmed the placement of the regions of interest. The hepatic PDFF determined from each infant was reported individually for free-breathing radial scan 1 and scan 2, and as an average of free-breathing radial scan 1 and scan 2.

Statistical analysis

Descriptive statistics, preparation time and scan time were reported as median ± interquartile range and range (minimum, maximum) or percentage (number). We compared differences in the distribution of liver image-quality scores between free-breathing radial scan 1, free-breathing radial scan 2, and Cartesian scans using McNemar-Bowker statistical tests for dependent categorical variables in STATA software version 12 (StataCorp, College Station, TX). A P-value <0.05 was considered significant. We assessed repeatability of free-breathing radial hepatic PDFF in MATLAB by calculating the mean difference, absolute mean difference, within-subject standard deviation, and coefficient of repeatability [51, 52] between back-to-back repeated scans (scan 1 and scan 2). Free-breathing radial VAT, SAT, BAT (volume and PDFF) and hepatic PDFF were calculated for all subjects and reported as median ± interquartile range and range (minimum, maximum) among subjects.

Results

Infant study population

Ten infants were enrolled in the study, and nine completed the entire study (90% completion rate). One infant completed only one free-breathing radial abdominal MRI scan because of crying. Characteristics for the study population are reported in Table 2. For ten infants, the median ± interquartile range and range (minimum, maximum) preparation time was 32±7 min (15 min, 81 min) and scan time was 24±11 min (15 min, 34 min), respectively (Table 3). Excluding the infant with the incomplete scan, the scan time was 24±11 min (20 min, 34 min). Of the ten infants, four were scanned without the anterior head coil attached.

Liver image quality

Representative axial and coronal reformat images of the liver with image-quality scores ranging 1–3 are shown in Fig. 2. Free-breathing radial images of the liver demonstrated higher image-quality scores than Cartesian abdominal images (P=0.011). Compared to free-breathing radial scan 1, free-breathing radial scan 2 showed a higher proportion of image-quality scores of 3 (89% vs. 30%, P=0.025). A summary of the proportion of free-breathing radial (scan 1 and scan 2) and Cartesian images receiving each score is shown in Table 4. One hundred percent of Cartesian images received non-diagnostic liver image-quality scores of 1 because of severe motion aliasing artifacts. In contrast, 0% of free-breathing radial (scan 1 and scan 2) abdominal images received liver image-quality scores of 1. Free-breathing radial images had minor motion artifacts that affected the liver less (image-quality score of 2) or no motion artifacts that affected the liver (image-quality score of 3).

Table 2 Subject characteristics

Characteristic	Infant subjects (n=10)
Age (months)	3.2±3.4, (2.3, 6.9)
Gender, male	50% (5)
Hispanic ethnicity	30% (3)
Race	
White	70% (7)
Asian	10% (1)
More than one race	20% (2)
Weight (kg)	7.0±1.6 (3.7, 9.9)
Height (cm)	59.6±7.9 (49.5, 69.9)

All information is reported as median ± interquartile range and range (minimum, maximum) or percentage (number)

Table 3 Infant characteristics and procedure times reported as median ± interquartile range and range (minimum, maximum) (n=10)

Subject	Preparation time (min)	Scan time (min)
1	26	20
2	15	21
3	34	24
4	33	24
5	30	33
6	30	27
7	47[a]	20
8	27[a]	32
9	35	15[b]
10	81	34
Median	31.5±7.0	24.0±10.5[c]
Range	(15, 81)	(15[b], 34)[c]

[a] Preparation of subject 8 was done during the scan of subject 7

[b] Incomplete scan

[c] The scan time excluding subject 9 with the incomplete scan was 24.0 ±11.0 (20, 34) min

Body composition analysis and hepatic PDFF quantification

VAT, SAT and BAT (volume and PDFF) and hepatic PDFF for all infants are listed in Table 5. The median ± interquartile range (minimum, maximum) number of slices used to contour SAT and VAT was 40±0 (32, 44), and in all subjects three slices were used to contour BAT. The median ± interquartile range (minimum, maximum) times to contour VAT, SAT and BAT were 92±57 min (42, 146), 20±8 min (10, 30) and 38 ±12 min (32, 70), respectively. PDFF maps from the infant with the lowest VAT, VAT-PDFF, SAT, SAT-PDFF, BAT and BAT-PDFF are shown in Fig. 3. This was a 2.5-month-old preterm boy born with intrauterine growth restriction. The hepatic PDFF for this boy (3.8%) was close to the median hepatic PDFF (3.4%). In contrast, PDFF maps from the infant with the highest hepatic PDFF (6.0%) are shown in Fig. 4. This 3.2-month-old infant had a family history notable for non-alcoholic fatty liver disease. Hepatic PDFF quantification using free-breathing radial abdominal scans demonstrated repeatability with mean difference = 0.21%, absolute mean difference = 0.56%, within-technique standard deviation = 0.69%, and coefficient of repeatability = 1.90%.

Discussion

In this study, quantification of body composition and hepatic fat in infants was feasible using free-breathing radial MRI. Moreover, free-breathing radial MRI had higher image quality in the liver compared to Cartesian MRI. Free-breathing radial quantification of hepatic PDFF demonstrated repeatability

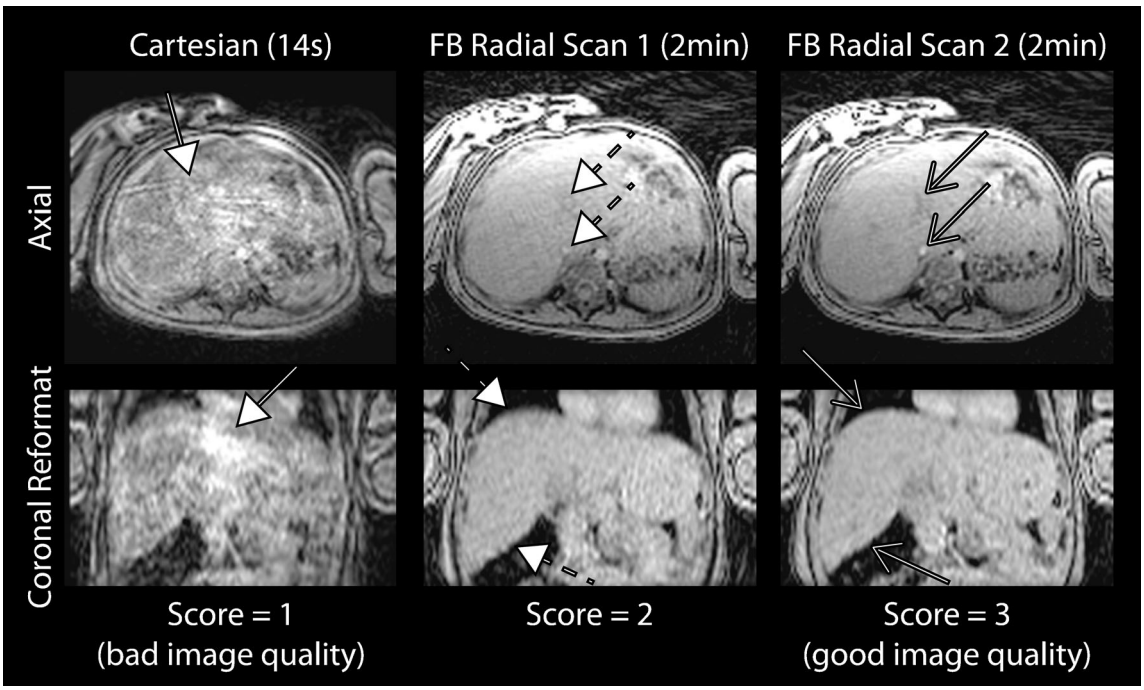

Fig. 2 Representative Cartesian and free-breathing radial infant abdominal MR images from subject 3, a 6.4-month-old girl. These examples have image-quality scores of 1–3. A score of 1 represents non-diagnostic images (i.e. bad image quality), a score of 2 represents diagnostic images with minor motion artifacts in the liver, and a score of 3 represents diagnostic images with no motion artifacts in the liver. Solid arrows indicate severe motion artifacts (score=1). Dashed arrows indicate small structures with minor motion blurring (score=2). Open arrows indicate small structures that appear sharp (score=3). *FB* free-breathing

Table 4 Summary of the image-quality scores

Score	Free-breathing radial scan 1[a,b] (n=10)	Free-breathing radial scan 2[a,b] (n=9)	Cartesian[a] (n=9)
1 (bad)	0.0%	0.0%	100.0%
2	70.0%	11.1%	0.0%
3 (good)	30.0%	88.9%	0.0%

Infant free-breathing abdominal MR images were scored for motion artifacts by a pediatric radiologist with 10+ years of experience using axial and coronal reformatted source images at the first echo time (TE=1.23 ms). Free-breathing radial scans (scan 1 and scan 2) were scored separately

[a] Statistically significant differences (P=0.011) in the distribution of image-quality scores between Cartesian and free-breathing radial scan 1 and scan 2

[b] Statistically significant differences (P=0.025) in the distribution of image-quality scores between free-breathing radial scan 1 and scan 2

with coefficient of repeatability <2%. Our technique allows for longitudinal studies and could be used to investigate the pathogenesis of and test interventions for metabolic diseases.

For all infants in our study population, the preparation time was approximately 30 min and scan time was approximately 25 min. The scan times in this study included the acquisition of two free-breathing radial abdominal scans, a free-breathing radial head and chest scan, and an additional Cartesian abdominal scan. For the infant with an incomplete MRI, only one free-breathing radial abdominal scan was acquired and the scan time was 15 min. In this study, all of the free-breathing radial abdominal, and head and chest scans were acquired with oversampling to ensure enough data were collected during the MRI exam. Therefore, the scan time reported in this study was longer than it would have been if the data had been acquired prospectively as fully sampled. If only a single fully sampled free-breathing radial abdominal scan is acquired, the scan time for the MRI exam can be reduced to approximately 15 min. Free-breathing radial imaging did not require sedation or anesthesia, thereby eliminating additional cost and time and potential complications.

Among the ten infants, the median ± interquartile range of hepatic PDFF was 3.4±1.1%. The results using our new free-breathing radial technique are consistent with previously reported hepatic PDFF values in infants [20, 21]. The infant with the highest hepatic PDFF in our cohort (6.0%) also had VAT and BAT volumes and BAT-PDFF that were among the highest compared to other infants. This infant's family history was notable for non-alcoholic fatty liver disease, and there was a maternal history of insulin resistance. Infants of diabetic mothers are at increased risk for metabolic syndrome [53, 54]. Previous studies reported significant differences in hepatic PDFF between infants born to mothers with gestational diabetes versus infants born to mothers without gestational diabetes. In these studies, hepatic PDFF positively correlated with maternal body mass index [20, 21]. It remains controversial whether NAFLD is an independent risk factor for metabolic syndrome [55]. However, large studies demonstrate an

Table 5 Infant hepatic fat and body composition measurements from free-breathing radial scans for the ten infant subjects

Subject	VAT (cm^3)	VAT-PDFF (%)	SAT (cm^3)	SAT-PDFF (%)	BAT (cm^3)	BAT-PDFF (%)	Hepatic PDFF (%) average (scan 1, scan 2)
1	36.0	39.9	385.9	89.6	1.0	26.1	4.0 (3.7, 4.3)
2	63.5	39.7	254.4	86.3	2.2	36.4	6.0 (5.9, 6.1)
3	48.2	43.9	324.6	88.2	2.4	44.2	2.4 (2.4, 2.3)
4	53.4	43.9	278.5	87.8	1.0	25.7	2.2 (2.8, 1.6)
5	61.6	40.5	256.8	85.1	1.5	22.0	2.8 (2.4, 3.3)
6	50.6	44.8	162.0	79.6	1.4	28.2	2.9 (2.4, 3.4)
7	17.0	34.2	148.4	77.8	0.7	17.3	3.8 (3.9, 3.7)
8	28.3	46.5	177.3	83.6	1.0	22.0	4.3 (4.0, 4.6)
9	69.8	37.7	469.6	90.2	N/A	N/A	3.5 (3.5, N/A)
10	53.8	44.7	358.2	93.0	1.8	37.7	3.3 (3.2, 3.4)
Median	52.0±20.7	42.2±4.7	267.7±153.2	87.1±5.3	1.4±0.7	26.1±14.4	3.4±1.1
Range	(17.0, 69.8)	(34.2, 46.5)	(148.4, 469.6)	(77.8, 93.0)	(0.7, 2.4)	(17.3, 44.2)	(2.2, 6.0)

Median ± interquartile range and range (minimum, maximum) among subjects is reported

BAT brown adipose tissue, *N/A* not available, *PDFF* proton-density fat fraction, *SAT* subcutaneous adipose tissue, *VAT* visceral adipose tissue

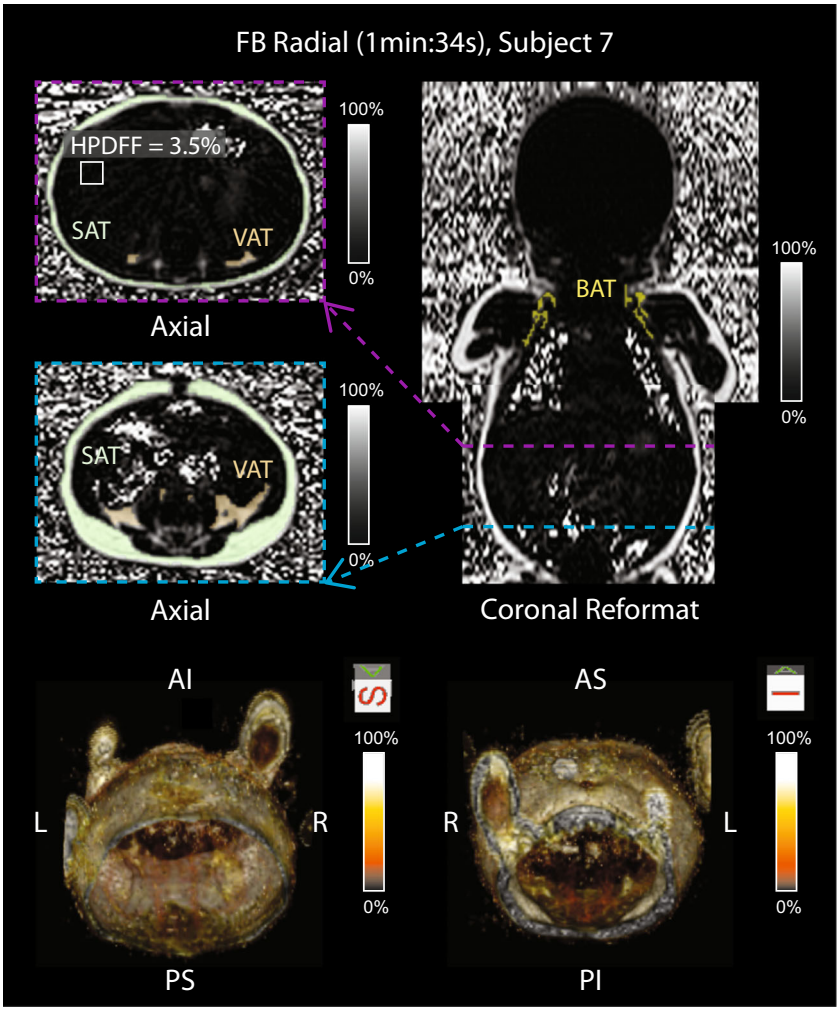

Fig. 3 Representative infant abdominal, and head and chest proton-density fat fraction (PDFF) maps (range: 0–100%) from subject 7, a 2.5-month-old boy. Abdominal PDFF maps are shown in axial and coronal reformat orientations. The head and chest PDFF map is shown in the coronal reformatted orientation. The coronal reformatted image was combined from the slabs acquired during the abdominal scan and the head and chest scan. Hepatic PDFF (*HPDFF*) in the liver is shown in a representative region of interest. Visceral adipose tissue (*VAT*) and subcutaneous adipose tissue (*SAT*) compartments are contoured on axial abdominal images. The brown adipose tissue (*BAT*) compartment is contoured on head and chest coronal reformatted images. In addition, 3-D rendered views of the abdominal PDFF map are displayed, with the orientations denoted as right (*R*), left (*L*), anterior-superior (*AS*), anterior-inferior (*AI*), posterior-superior (*PS*) and posterior-inferior (*PI*). This boy was born preterm with intrauterine growth restriction. He had the lowest VAT volume (17.0 cm^3), VAT-PDFF (34.2%), SAT volume (148.4 cm^3), SAT-PDFF (77.8%), BAT volume (0.7 cm^3) and BAT-PDFF (17.3%) in the study cohort. *FB* free-breathing

association between NAFLD and metabolic syndrome in children [56]. Further research in a larger cohort of infants will be required to investigate hepatic PDFF in infancy and the relationship between hepatic PDFF, NAFLD and future metabolic syndrome.

The characterization of VAT and BAT are important for improving the understanding and management of metabolic syndrome [10–13, 15, 20, 36]. Excessive WAT in infancy is linked to later onset of metabolic syndrome [10, 14, 15, 20]. Beyond the newborn period, larger volumes of BAT in infants, children and young adults are associated with a decreased risk of metabolic syndrome [10, 12, 13, 16]. Furthermore, it has been speculated that lower BAT fat content (PDFF) in infants and children might be associated with a decreased risk for metabolic syndrome later in life [11–13]. Interestingly, in our study, an infant who was born preterm with intrauterine growth restriction had the lowest VAT, SAT and BAT (volume and PDFF) compared to the other infants. The clinical significance of these findings remains unknown. Moreover, in this study we did not measure lean body mass, a key component of body composition. Larger increases in lean body mass have been associated with smaller decreases in BAT [36]. Infants born preterm, small for gestational age, large for gestational age, and with intrauterine growth restriction have increased insulin production and decreased insulin sensitivity and lean body mass [17, 57–59]. When these infants experience rapid weight gain in early childhood, there is an increased risk for later metabolic syndrome

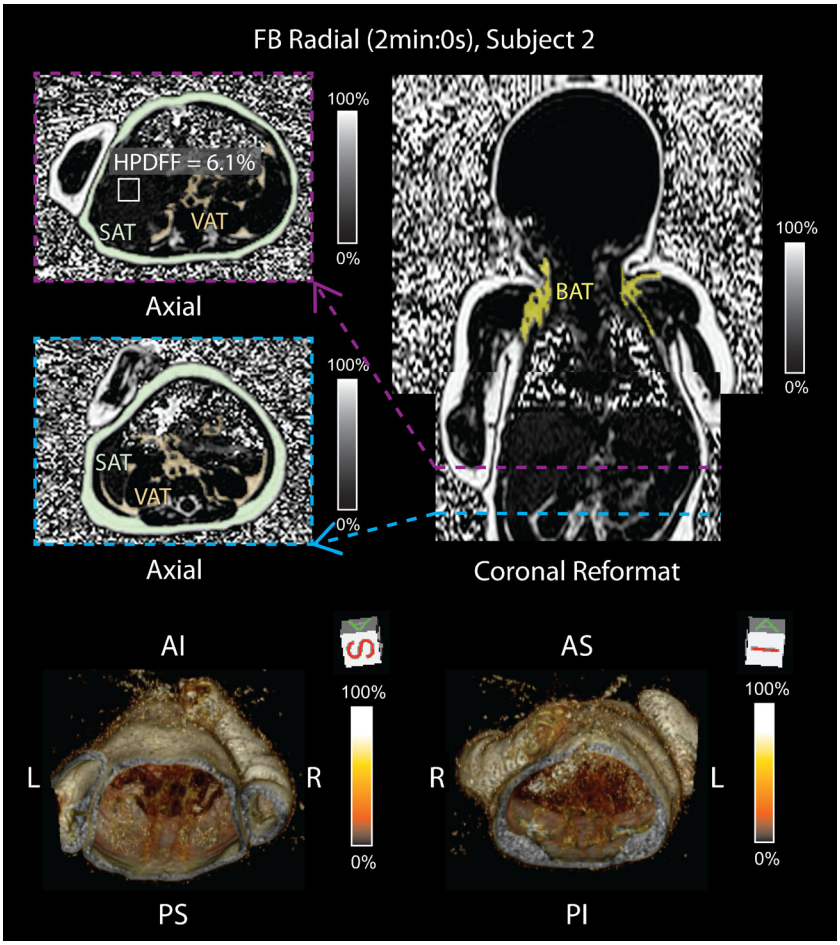

Fig. 4 Representative infant abdominal, and head and chest proton-density fat fraction (PDFF) maps (range: 0–100%) from subject 2, a 3.2-month-old boy. Abdominal PDFF maps are shown in axial and coronal reformat orientations. The head and chest PDFF map is shown in the coronal reformatted orientation. The coronal reformatted image was combined from the slabs acquired during the abdominal scan and the head and chest scan. Hepatic PDFF (*HPDFF*) in the liver is shown in a representative region of interest. Visceral adipose tissue (*VAT*) and subcutaneous adipose tissue (*SAT*) compartments are contoured on axial abdominal images. The brown adipose tissue (*BAT*) compartment is contoured on head and chest coronal reformatted images. In addition, 3-D rendered views of the abdominal PDFF map are displayed, with the orientations denoted as right (*R*), left (*L*), anterior-superior (*AS*), anterior-inferior (*AI*), posterior-superior (*PS*) and posterior-inferior (*PI*). This boy was born full term and had a family history of non-alcoholic fatty liver disease. He had the highest HPDFF (6.0%), second highest VAT volume (63.5 cm^3), second highest BAT volume (2.2 cm^3), and third highest BAT-PDFF (36.4%) in the study cohort. *FB* free-breathing

[17, 60, 61]. Additional work is needed to decipher the relationship between maternal, fetal and neonatal body composition (volume and content) and hepatic PDFF with metabolic syndrome.

Previous studies in newborns with a mean age <2 weeks observed abdominal VAT ranging from 11 cm^3 to 44 cm^3, and SAT ranging from 50 cm^3 to 159 cm^3 [15, 20, 31]. Compared to our results, VAT and SAT volumes observed in these newborn studies were lower than the volumes we observed in our study (median VAT=52.0 cm^3, median SAT=267.7 cm^3). This most likely reflects age differences. Other studies in infants with a mean age of approximately 2 months reported total body VAT and SAT measurements. Hence VAT and SAT volumes observed in these studies were higher than the values we obtained because these volumes were measured from total body fat rather than abdominal fat alone [62].

Two-echo and six-echo Cartesian chemical-shift-encoded MRI techniques have been used to quantify fat content [11, 12, 16, 32, 35]. Two-echo techniques do not correct for confounding factors, such as the multi-peak spectrum of fat, and might underestimate PDFF [62]. On the other hand, six-echo techniques correct for confounding factors, including the multi-peak spectrum of fat [62]. BAT-PDFF and SAT-PDFF reported in our study were similar to those in studies of infants with a mean age of 1–2 months [11, 12, 16]. Of these studies, two used a two-echo chemical-shift-encoded MRI technique [12, 16] and did not correct for confounding factors, which might underestimate PDFF [62]. Our study, along with another study [11], used a six-echo chemical-shift-encoded MRI technique that corrects for confounding factors. Determining fat content for body composition by accurate quantification of PDFF might be clinically relevant. Evidence suggests that a

lower BAT-PDFF during infancy is associated with a lower risk of metabolic syndrome [11, 13]. Lower PDFF might indicate increased metabolism of fat to produce heat, a process known as non-shivering thermogenesis that is important for preventing hypothermia [10–13]. Fat with a higher PDFF might function more like WAT, while fat with a lower PDFF might function more like BAT [11–13]. Our PDFF results are consistent with these studies; in our study median VAT-PDFF was higher than median BAT-PDFF (42.2% versus 26.1%).

Compared to free-breathing radial scan 1, free-breathing radial scan 2 showed a higher proportion of liver image-quality scores of 3 (89% vs. 30%, P=0.025). These differences could be a result of more motion, irregular breathing or heavy breathing during free-breathing radial scan 1 compared to scan 2. Free-breathing radial imaging was typically performed first during the MRI exam. At the beginning of the scan, we observed that infants were often startled and cried. We believe this is most likely secondary to the noises generated by the MRI. Soon after, infants usually stopped crying, fell asleep, and moved less as the exam progressed. Hence during free-breathing radial scan 2, infants might have fallen into a deeper sleep and moved less compared to free-breathing radial scan 1. In this study, no self-navigation, respiratory gating or motion compensation was performed. Free-breathing radial imaging can be used to generate a self-navigation signal, which could be incorporated in future work to further improve image quality [63–65].

The practicality of infant MRI scanning should be considered. First, MRI is expensive compared to other imaging modalities. This limits access to infant MRI for research and clinical purposes. Second, MRI is loud because of the rapidly changing gradients [66]. To reduce noise and avoid hearing damage during the MRI exam, earplugs and earmuffs are required. Third, MRI can produce heating in the subject, characterized in terms of the specific absorption rate [66]. To reduce the specific absorption rate, we used a low flip angle of 5° for the free-breathing radial and Cartesian acquisitions to produce a low whole-body specific absorption rate of 0.08–0.10 W/kg and B_{1+rms} of 0.6 μT. Finally, abdominal body composition analysis is time-consuming and requires training. In this study, the median time for contouring VAT, SAT and BAT was approximately 90 min, 20 min and 40 min, respectively.

This study has limitations. First, the sample size was small and the range of hepatic PDFF in this population was narrow. Larger sample sizes with a wider range of hepatic PDFF and longitudinal studies are needed to elucidate associations between hepatic PDFF, VAT, SAT and BAT (volume and PDFF), and demographics, clinical data and risk factors for metabolic syndrome. Second, BAT can be present in other regions besides the supraclavicular and axillary regions, such as the cervical, paravertebral, perirenal and periadrenal regions. Because supraclavicular fat is considered the largest depot of brown fat in infants [67], we chose to measure the supraclavicular along with the axillary region for BAT. We were unable to validate that all fat in the supraclavicular region was BAT. To do this, a biopsy or positron emission tomography (PET), which uses radiation [22, 67], would be required. Because this technique was evaluated in a research setting, these confirmatory procedures were not possible. In previous work, autopsies have confirmed that voxels with intermediate quantitative MRI PDFF values reflect BAT [67]. Third, we did not compare our hepatic fat results to the gold standard, liver biopsy, or a breath-held Cartesian scan. Performing a liver biopsy for research purposes in healthy infants is unethical. Breath-held MRI scans were not possible in this study because infants cannot voluntarily perform a breath-hold and sedation was not used. However, we assessed the repeatability of free-breathing radial imaging for hepatic fat quantification and our technique demonstrated repeatability with coefficient of repeatability <2%. Furthermore, previous studies in a fat phantom, adults and children have demonstrated agreement in quantitative PDFF between free-breathing radial MRI, breath-holding Cartesian MRI and breath-holding MRS [42, 43]. Fourth, we did not analyze repeatability for abdominal body composition because of the lengthy analysis time. Head and chest scans were not repeated because of scan time considerations. However all of our measurements were consistently performed by one coordinator and verified by a radiologist. Fifth, preparation for infant MRI can be time-consuming and requires staff training and parental education. We demonstrated that with training the median preparation time and scan time for an infant MRI exam were approximately 32 min and 24 min, respectively. Finally, this study required the infant to be asleep or calm during the MRI exam. If the infant began to cry during the MRI exam, the exam could be incomplete. While our new free-breathing radial technique is robust to breathing motion, additional corrections might be needed for severe motion. To improve the motion robustness of our free-breathing radial technique, motion detection using a self-navigation signal might be used to characterize and compensate for severe motion [63–65], which could be explored in future studies.

Conclusion

Free-breathing 3-D quantification of infant body composition and hepatic fat is feasible using a free-breathing radial MRI technique within a median scan time of 24 min and might be reduced to within 15 min if only a single free-breathing radial abdominal scan is required. Free-breathing radial MRI demonstrated improved liver image quality compared to conventional Cartesian MRI and quantified hepatic PDFF with repeatability of mean difference <0.25% and coefficient of repeatability <2%. The new free-breathing radial MRI technique

might help unravel the early origins of metabolic diseases by providing accurate and detailed information about body composition and hepatic fat in infants.

Acknowledgments Research reported in this publication was supported in part by a UCLA Radiology Department Exploratory Research Grant (#16-0002). The authors thank Aaron Scheffler, Dr. Joanna Yeh, Tammy Floore, Glen Nyborg and Sergio Godinez at UCLA for their help with this project. This work acknowledges the use of the ISMRM Fat-Water Toolbox (http://ismrm.org/workshops/FatWater12/data.htm).

Compliance with ethical standards

Conflicts of interest The first author and corresponding author receive institutional research support from Siemens Healthineers. However, this study was not supported by Siemens.

Appendix: Detailed procedures for infant preparation and MRI experiments

Preparation for the MRI exam began with the recruitment and consenting process. Prior to the MRI exam, the study team contacted the parents several times by email or phone to provide them with detailed information about what an MRI is and what to expect for the MRI exam. During this time, we gave parents a picture or video of the MRI and a chance to discuss the MRI procedure in detail with the study team. We also gave the parents instructions on how to prepare for the MRI exam and contacted them to go over the instructions prior to the MRI exam. On the day of the exam, parents were asked to dress their infant in clothing with 100% cotton to ensure that there was no metal. If the parents had any 100% cotton blankets or items to help calm the infant, such as a pacifier or toy, they were asked to bring them as long as the items did not contain metal. Parents were instructed to arrive 30–45 min before their scheduled scan time so that there was sufficient time to consent and prepare for the scan. The preparation steps in Fig. 1 began after the parents and infants arrived and consented to the exam. Some of the preparation steps in Fig. 1 can begin before the MRI scanner becomes available.

We started recording preparation time when the infant and parent/legal guardian entered the MRI suite. First, infants were checked to ensure their wardrobe contained no metal. If the parents brought items to calm the infant during the scan, these items were tested for metal with a magnet prior to bringing them into the MRI room. The infants were breast or bottle fed, swaddled and rocked to a sleepy state (Fig. 1). The infant's caregivers were involved in the feeding and swaddling of the infant. Earplugs and earmuffs were placed on the infant for hearing protection (Fig. 1). Infants were then placed on a vacuum immobilizer and the clips on the immobilizer were fastened (Fig. 1). To limit set-up procedures that might cause discomfort to the infant, we did not use the head Velcro strap and vacuum pump to remove air from the vacuum immobilizer. The posterior head coil was then positioned and the infant was placed on the MRI table (Fig. 1). Cloths were placed between the infant's ears and the head coil to immobilize the head and attenuate MRI noise. Prior to attaching the body matrix array, blankets were placed on both sides of the infant to prop up the body matrix array so that it did not touch the infant and to reduce bulk motion (Fig. 1). Finally, the anterior portion of the head coil was attached (Fig. 1). If the infant began crying when the coil was attached, the anterior portion of the head coil was removed. After all the coils were positioned, the MRI table and the infant were advanced into the MRI bore and the total preparation time was recorded. A diagram of infant preparation procedures is shown in Fig. 1.

After advancing the infant and the MRI table into the bore, the start time for the scan was recorded. For each infant, one parent/legal guardian stayed in the MRI room and communicated with the technologist during the scan. If the infant began crying, the caregivers were allowed to comfort the infant by touching their feet and checking on them. If the infant did not stop crying or the parent/legal guardian asked to stop the scan, the infant was removed from the scanner and comforted in the immobilizer. If the infant then settled down, the infant was placed on the MRI table again and set-up procedures on the MRI table were repeated. The total scan time was calculated after the MRI scan protocol was completed.

References

1. Karnik S, Kanekar A (2012) Childhood obesity: a global public health crisis. Int J Prev Med 3:1–7
2. Kim CH, Younossi ZM (2008) Nonalcoholic fatty liver disease: a manifestation of the metabolic syndrome. Cleve Clin J Med 75: 721–728
3. Sundaram SS, Zeitler P, Nadeau K (2009) The metabolic syndrome and nonalcoholic fatty liver disease in children. Curr Opin Pediatr 21:529–535
4. Paschos P, Paletas K (2009) Non alcoholic fatty liver disease and metabolic syndrome. Hippokratia 13:9–19
5. Fabbrini E, Magkos F, Mohammed BS et al (2009) Intrahepatic fat, not visceral fat, is linked with metabolic complications of obesity. Proc Natl Acad Sci 106:15430–15435
6. Lonardo A, Ballestri S, Marchesini G et al (2015) Nonalcoholic fatty liver disease: a precursor of the metabolic syndrome. Dig Liver Dis 47:181–190
7. Uppal V, Mansoor S, Furuya KN (2016) Pediatric non-alcoholic fatty liver disease. Curr Gastroenterol Rep 18:24
8. Nobili V, Svegliati-Baroni G, Alisi A et al (2013) A 360-degree overview of paediatric NAFLD: recent insights. J Hepatol 58: 1218–1229
9. Vernon G, Baranova A, Younossi ZM (2011) Systematic review: the epidemiology and natural history of non-alcoholic fatty liver disease and non-alcoholic steatohepatitis in adults. Aliment Pharmacol Ther 34:274–285
10. Gesta S, Tseng YH, Kahn CR (2007) Developmental origin of fat: tracking obesity to its source. Cell 131:242–256

11. Hu HH, Yin L, Aggabao PC et al (2013) Comparison of brown and white adipose tissues in infants and children with chemical-shift-encoded water-fat MRI. J Magn Reson Imaging 38:885–896
12. Entringer S, Rasmussen J, Cooper DM et al (2017) Association between supraclavicular brown adipose tissue composition at birth and adiposity gain from birth to 6 months of age. Pediatr Res 82: 1017–1021
13. Deng J, Schoeneman SE, Zhang H et al (2015) MRI characterization of brown adipose tissue in obese and normal-weight children. Pediatr Radiol 45:1682–1689
14. Toomey CM, Cremona A, Hughes K et al (2015) A review of body composition measurement in the assessment of health. Top Clin Nutr 30:16–32
15. Modi N, Thomas EL, Uthaya SN et al (2009) Whole body magnetic resonance imaging of healthy newborn infants demonstrates increased central adiposity in Asian Indians. Pediatr Res 65:584–587
16. Rasmussen JM, Entringer S, Nguyen A et al (2013) Brown adipose tissue quantification in human neonates using water-fat separated MRI. PLoS One 8:e77907
17. Calkins K, Devaskar SU (2011) Fetal origins of adult disease. Curr Probl Pediatr Adolesc Health Care 41:158–176
18. Wesolowski SR, El Kasmi KC, Jonscher KR, Friedman JE (2016) Developmental origins of NAFLD: a womb with a clue. Nat Rev Gastroenterol Hepatol 14:81–96
19. Brumbaugh DE, Friedman JE (2014) Developmental origins of nonalcoholic fatty liver disease. Pediatr Res 75:140–147
20. Modi N, Murgasova D, Ruager-Martin R et al (2011) The influence of maternal body mass index on infant adiposity and hepatic lipid content. Pediatr Res 70:287–291
21. Brumbaugh DE, Tearse P, Cree-Green M et al (2013) Intrahepatic fat is increased in the neonatal offspring of obese women with gestational diabetes. J Pediatr 162:930–936.e1
22. Toro-Ramos T, Paley C, Pi-Sunyer FX, Gallagher D (2015) Body composition during fetal development and infancy through the age of 5 years. Eur J Clin Nutr 69:1279–1289
23. Thayyil S, Cleary JO, Sebire NJ et al (2009) Post-mortem examination of human fetuses: a comparison of whole-body high-field MRI at 9·4 T with conventional MRI and invasive autopsy. Lancet 374:467–475
24. Lee SY, Gallagher D (2008) Assessment methods in human body composition. Curr Opin Clin Nutr Metab Care 11:566–572
25. Shuster A, Patlas M, Pinthus JH, Mourtzakis M (2012) The clinical importance of visceral adiposity: a critical review of methods for visceral adipose tissue analysis. Br J Radiol 85:1–10
26. Sumida Y, Nakajima A, Itoh Y (2014) Limitations of liver biopsy and non-invasive diagnostic tests for the diagnosis of nonalcoholic fatty liver disease/nonalcoholic steatohepatitis. World J Gastroenterol 20:475–485
27. Shen W, Liu H, Punyanitya M et al (2005) Pediatric obesity phenotyping by magnetic resonance methods. Curr Opin Clin Nutr Metab Care 8:595–601
28. Lee SS, Park SH (2014) Radiologic evaluation of nonalcoholic fatty liver disease. World J Gastroenterol 20:7392–7402
29. Bellentani S, Marino M (2009) Epidemiology and natural history of non-alcoholic fatty liver disease (NAFLD). Ann Hepatol 8:S4–S8
30. Loomba R, Sirlin CB, Schwimmer JB, Lavine JE (2009) Advances in pediatric nonalcoholic fatty liver disease. Hepatology 50:1282–1293
31. Harrington TAM, Thomas EL, Frost G et al (2004) Distribution of adipose tissue in the newborn. Pediatr Res 55:437–441
32. Yu NY, Wolfson T, Middleton MS et al (2017) Bone marrow fat content is correlated with hepatic fat content in paediatric non-alcoholic fatty liver disease. Clin Radiol 72:425.e9–425.e14
33. Reeder SB, Hu HH, Sirlin CB (2012) Proton density fat-fraction: a standardized MR-based biomarker of tissue fat concentration. J Magn Reson Imaging 36:1011–1014
34. Olhager E, Flinke E, Hannerstad U, Forsum E (2003) Studies on human body composition during the first 4 months of life using magnetic resonance imaging and isotope dilution. Pediatr Res 54: 906–912
35. Dyke JP, Garfinkel AC, Groves AM, Kovanlikaya A (2018) High-resolution rapid neonatal whole-body composition using 3.0 tesla chemical shift magnetic resonance imaging. Pediatr Res 83:638–644
36. Ponrartana S, Aggabao PC, Chavez TA et al (2016) Changes in brown adipose tissue and muscle development during infancy. J Pediatr 173:116–121
37. Haney B, Reavey D, Atchison L et al (2010) Magnetic resonance imaging studies without sedation in the neonatal intensive care unit: safe and efficient. J Perinat Neonatal Nurs 24:256–266
38. Golan A, Marco R, Raz H, Shany E (2011) Imaging in the newborn: infant immobilizer obviates the need for anesthesia. Isr Med Assoc J 13:663–665
39. Mathur AM, Neil JJ, McKinstry RC, Inder TE (2008) Transport, monitoring, and successful brain MR imaging in unsedated neonates. Pediatr Radiol 38:260–264
40. Windram J, Grosse-Wortmann L, Shariat M et al (2012) Cardiovascular MRI without sedation or general anesthesia using a feed-and-sleep technique in neonates and infants. Pediatr Radiol 42:183–187
41. Winkelmann S, Schaeffter T, Koehler T et al (2007) An optimal radial profile order based on the golden ratio for time-resolved MRI. IEEE Trans Med Imaging 26:68–76
42. Armstrong T, Dregely I, Stemmer A et al (2018) Free-breathing liver fat quantification using a multiecho 3D stack-of-radial technique. Magn Reson Med 79:370–382
43. Armstrong T, Ly KV, Murthy S et al (2018) Free-breathing quantification of hepatic fat in healthy children and children with nonalcoholic fatty liver disease using a multi-echo 3-D stack-of-radial MRI technique. Pediatr Radiol 48:941–953
44. Zhong X, Nickel MD, Kannengiesser SAR et al (2014) Liver fat quantification using a multi-step adaptive fitting approach with multi-echo GRE imaging. Magn Reson Med 72:1353–1365
45. Breuer FA, Blaimer M, Heidemann RM et al (2005) Controlled aliasing in parallel imaging results in higher acceleration (CAIPIRINHA) for multi-slice imaging. Magn Reson Med 53: 684–691
46. Ren J, Dimitrov I, Sherry AD, Malloy CR (2008) Composition of adipose tissue and marrow fat in humans by 1H NMR at 7 tesla. J Lipid Res 49:2055–2062
47. Hernando D, Kellman P, Haldar JP, Liang Z-P (2010) Robust water/fat separation in the presence of large field inhomogeneities using a graph cut algorithm. Magn Reson Med 63:79–90
48. Gleich DF (2009) Models and algorithms for pagerank sensitivity. Doctoral dissertation, Stanford University, Stanford
49. International Society for Magnetic Resonance in Medicine (2012) ISMRM fat-water toolbox. https://www.ismrm.org/workshops/FatWater12/data.htm. Accessed 22 Feb 2019
50. Liu CY, McKenzie CA, Yu H et al (2007) Fat quantification with IDEAL gradient echo imaging: correction of bias from T1 and noise. Magn Reson Med 58:354–364
51. Bartlett JW, Frost C (2008) Reliability, repeatability and reproducibility: analysis of measurement errors in continuous variables. Ultrasound Obstet Gynecol 31:466–475
52. Obuchowski NA, Reeves AP, Huang EP et al (2014) Quantitative imaging biomarkers: a review of statistical methods for computer algorithm comparisons. Stat Methods Med Res 24:68–106
53. Leddy MA, Power ML, Schulkin J (2008) The impact of maternal obesity on maternal and fetal health. Rev Obstet Gynecol 1:170–178

54. Gillman MW, Rifas-Shiman S, Berkey CS et al (2003) Maternal gestational diabetes, birth weight, and adolescent obesity. Pediatrics 111:e221–e226
55. Yang KC, Hung H-F, Lu C-W et al (2016) Association of non-alcoholic fatty liver disease with metabolic syndrome independently of central obesity and insulin resistance. Sci Rep 6:27034
56. Schwimmer JB, Pardee PE, Lavine JE et al (2008) Cardiovascular risk factors and the metabolic syndrome in pediatric nonalcoholic fatty liver disease. Circulation 118:277–283
57. Boney CM, Verma A, Tucker R, Vohr BR (2005) Metabolic syndrome in childhood: association with birth weight, maternal obesity, and gestational diabetes mellitus. Pediatrics 115:e290–e296
58. Newton KP, Feldman HS, Chambers CD et al (2017) Low and high birth weights are risk factors for nonalcoholic fatty liver disease in children. J Pediatr 187:141–146.e1
59. Nobili V, Marcellini M, Marchesini G et al (2007) Intrauterine growth retardation, insulin resistance, and nonalcoholic fatty liver disease in children. Diabetes Care 30:2638–2640
60. Breij LM, Kerkhof GF, Hokken-Koelega ACS (2015) Risk for non-alcoholic fatty liver disease in young adults born preterm. Horm Res Paediatr 84:199–205
61. Faienza MF, Brunetti G, Ventura A et al (2013) Nonalcoholic fatty liver disease in prepubertal children born small for gestational age: influence of rapid weight catch-up growth. Horm Res Paediatr 79:103–109
62. Reeder SB, Cruite I, Hamilton G, Sirlin CB (2011) Quantitative assessment of liver fat with magnetic resonance imaging and spectroscopy. J Magn Reson Imaging 34:729–749
63. Armstrong T, Ly KV, Wang Y, Martin T, Ghahremani S, Sung K, Calkins KL, Wu HH (2018) Free-breathing hepatic fat quantification in children and infants using a 3D stack-of-radial technique: assessment of accuracy and repeatability. In: Proceedings of the 26th Annual Meeting of ISMRM, Paris, France, p 522
64. Benkert T, Fend L, Sodickson DK et al (2017) Free-breathing volumetric fat/water separation by combining radial sampling, compressed sensing, and parallel imaging. Magn Reson Med 78:565–576
65. Feng L, Axel L, Chandarana H et al (2016) XD-GRASP: golden-angle radial MRI with reconstruction of extra motion-state dimensions using compressed sensing. Magn Reson Med 75:775–788
66. Sammet S (2016) Magnetic resonance safety. Abdom Radiol 41:444–451
67. Hu HH, Tovar JP, Pavlova Z et al (2012) Unequivocal identification of brown adipose tissue in a human infant. J Magn Reson Imaging 35:938–942